Gazi Üniversitesi
Fen Bilimleri Dergisi
PART C: TASARIM VE TEKNOLOJİ

Gazi University
Journal of Science
PART C: DESIGN AND TECHNOLOGY

GU J Sci, Part C, 14(3): 1225-1239 (2026)

Solid-State Synthesis of High Voltage Cathode Active Material: Taguchi Optimization of Ball Milling and Structural Impact of Boron Doping

Yunus Emre GUL[1], Humza ASHRAF[2], Billur Deniz KARAHAN[1*].

[1] *Istanbul Technical University, Department of Metallurgical and Materials Engineering, Istanbul, Turkey*

[2] *Istanbul Medipol University, Biomedical Engineering & Bioinformatics, Istanbul, Turkey*

Article Info

Research article
Received: 27/12/2025
Revision: 16/02/2026
Accepted: 16/03/2026

Keywords

Spinel LNMO
Boron dopping
Solid state synthesis
High voltage cathode
Lithium-ion batteries

Makale Bilgisi

Araştırma makalesi
Başvuru: 27/12/2025
Düzeltme: 16/02/2026
Kabul: 16/03/2026

Anahtar Kelimeler

Spinel Yapılı LNMO
Bor Katkılama
Katı Hal Sentezi Kama
Yüksek Voltajlı Katot
Lityum-İyon Piller

Graphical/Tabular Abstract (Grafik Özet)

Boron-doped LNMO cathodes optimized via Taguchi-designed solid-state ball milling exhibited enhanced structural stability and delivered 110 mAh g⁻¹ with excellent capacity retention (97.5 mAh g⁻¹ after 130 cycles) (Taguchi deney tasarımı ile optimize edilen katı hâl bilyalı öğütme yöntemiyle sentezlenen bor katkılı LNMO katotları, gelişmiş yapısal kararlılık göstererek 110 mAh g⁻¹ kapasite ve 130 çevrim sonunda 97.5 mAh g⁻¹ kapasite koruması sağlamıştır.)

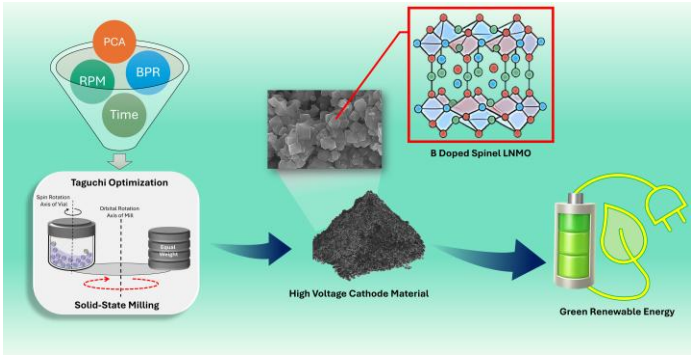

Figure A*: Graphical abstract of synthesis of B dopped LNMO cathode material/*
Şekil A: *B katkılı LNMO katot malzemesinin sentezine ait grafik özeti*

Highlights (Önemli noktalar)

- *Taguchi optimized solid-state synthesis of high-performance B-doped LNMO. /Yüksek performanslı B-katkılı LNMO'nun Taguchi yöntemiyle optimize edilmiş katı hal sentezi.*
- *B-LNMO delivered 97.5 mAh g⁻¹ after 130 cycles. /B-LNMO, 130 çevrimden sonra 97,5 mAh g⁻¹ değerini sağladı.*
- *B-LNMO at 800 °C calcination process enhanced the structural stability and cycling performance. /800 °C'deki B-LNMO kalsinasyon işlemi, yapısal kararlılığı ve çevrim performansını iyileştirdi.*

Aim (Amaç): *The study aims to synthesize B-doped LNMO cathode via a solid-state method, with parameters optimized using the L9 Taguchi experimental design. /Bu çalışma, L9 Taguchi deneysel tasarım yöntemiyle optimize edilen parametreler kullanılarak, katı hal yöntemiyle B-katkılı LNMO katodu sentezlemeyi amaçlamaktadır)*

Originality (Özgünlük): *This study is the first to apply the Taguchi L9 design to optimize the solid-state synthesis of B-doped LNMO, using the "larger-is-better" approach to maximize the first discharge capacity. /Bu çalışma, B katkılı LNMO'nun katı hâl sentez parametrelerini optimize etmek için Taguchi L9 deney tasarımını ilk kez uygulamış ve proses koşullarını ilk deşarj kapasitesini en üst düzeye çıkarmak amacıyla "büyük olan daha iyidir (larger-is-better)" yaklaşımıyla optimize etmiştir.*

Results (Bulgular): *The Taguchi-optimized B-doped LNMO delivered an initial discharge capacity of 110 mAh g⁻¹ and retained 97.5 mAh g⁻¹ after 130 cycles, demonstrating excellent electrochemical performance. /Taguchi ile optimize edilen bor katkılı LNMO, 110 mAh g⁻¹ başlangıç deşarj kapasitesi ve 130 çevrim sonunda 97.5 mAh g⁻¹ kapasite koruması ile üstün elektrokimyasal performans göstermiştir.*

Conclusion (Sonuç): *Taguchi optimization identified BPR, milling speed, and milling time as key factors, while 1% B doping improved LNMO stability and capacity retention. /Taguchi optimizasyonu, BPR, öğütme hızı ve öğütme süresini temel parametreler olarak belirlerken, %1 bor katkısı LNMO'nun kararlılığını ve kapasite korunumunu artırmıştır.*

*Corresponding author, e-mail: bdkarahan@itu.edu.tr
DOI: 10.29109/gujsc.1850067

GU J Sci, Part C, 14(3): 1225-1239 (2026)

Gazi Üniversitesi
Fen Bilimleri Dergisi
PART C: TASARIM VE TEKNOLOJİ

Gazi University
Journal of Science
PART C: DESIGN AND TECHNOLOGY

http://dergipark.gov.tr/gujsc

Solid-State Synthesis of High Voltage Cathode Active Material: Taguchi Optimization of Ball Milling and Structural Impact of Boron Doping

Yunus Emre GUL[1], Humza ASHRAF[2], Billur Deniz KARAHAN[1*].

[1] *Istanbul Technical University, Department of Metallurgical and Materials Engineering, Istanbul, Turkey*

[2] *Istanbul Medipol University, Biomedical Engineering & Bioinformatics, Istanbul, Turkey*

Article Info

Research article
Received: 27/12/2025
Revision: 16/02/2026
Accepted: 16/03/2026

Keywords

Spinel LNMO
Boron dopping
Solid state synthesis
High voltage cathode
Lithium-ion batteries

Abstract

The cost-performance trade-off is a critical factor in developing new cathode materials. Among several commercially available chemistries, lithium nickel manganese oxide (LNMO) a high-voltage, cobalt-free and low-nickel chemistry, offers a promising solution in this context. In this study, boron doped micron-sized spinel LNMO is synthesized via solid-state ball milling, by optimizing milling parameters via L_9 (3^4) Taguchi design. The effects of 1% boron doping and calcination temperature (800 and 900 °C) on the structural stability and electrochemical performance of the material are investigated. The sample being milled at 400 rpm with a 5:1 BPR for 12 hours and calcined at 800 °C delivers an initial capacity of 110 mAh g^{-1}, and it retains 97.5 mAh g^{-1} after 130 cycles at 0.1C (1C = 147 mA g^{-1}). The capacity retention is attributed to the strengthened B–O bonding, which enhances structural stability, while calcination at 800 °C effectively minimizes particle agglomeration and facilitates the phase transformation. These results demonstrate the synergistic effects of processing optimization and boron doping on LNMO cathode performance, offering valuable insights for the advancement of lithium-ion electrode active materials.

Yüksek Voltajlı Katot Aktif Malzemesinin Katı Hal Sentezi: Bilyalı Öğütmenin Taguchi Optimizasyonu ve Bor Katkılamasının Yapısal Etkisi

Makale Bilgisi

Araştırma makalesi
Başvuru: 27/12/2025
Düzeltme: 16/02/2026
Kabul: 16/03/2026

Anahtar Kelimeler

Spinel Yapılı LNMO
Bor Katkılama
Katı Hal Sentezi Kama
Yüksek Voltajlı Katot
Lityum-İyon Piller

Özet

Maliyet-performans dengesi, yeni katot malzemelerinin geliştirilmesinde kritik bir faktördür. Ticari olarak mevcut çeşitli katot kimyaları arasında, yüksek voltajlı, kobalt içermeyen ve düşük nikel içerikli bir katot malzemesi olan lityum nikel mangan oksit (LNMO) bu açıdan umut verici bir çözüm sunmaktadır. Bu çalışmada, bor katkılı mikron boyutlu spinel LNMO, öğütme parametrelerinin L9 (3^4) Taguchi deney tasarımı kullanılarak optimize edildiği katı hal bilyalı öğütme yöntemi ile sentezlenmiştir. Yapıya %1 oranında bor katkılanmasının ve 800 °C ile 900 °C kalsinasyon sıcaklıklarının malzemenin yapısal kararlılığı ve elektrokimyasal performansı üzerindeki etkileri incelenmiştir. 400 rpm hızda, 5:1 bilye-toz oranında (BPR) ve 12 saat süreyle öğütülen, ardından 800 °C'de kalsine edilen numune, başlangıçta 110 mAsa g^{-1} kapasitesi sergilemiş ve 0.1C akım yoğunluğunda (1C = 147 mA g^{-1}) gerçekleştirilen 130 çevrim sonrasında 97.5 mAsa g^{-1} kapasiteyi korumuştur. Elde edilen yüksek kapasite korunumu, yapısal kararlılığı artıran güçlendirilmiş B–O bağlarına atfedilmektedir. Ayrıca, 800 °C'de gerçekleştirilen kalsinasyon işlemi, parçacık aglomerasyonunu etkin şekilde azaltmış ve faz dönüşümünü desteklemiştir. Sonuçlar, işlem parametrelerinin optimizasyonu ile bor katkılamasının LNMO katot performansı üzerinde sinerjik bir etki yarattığını göstermekte ve lityum-iyon pil elektrot aktif malzemelerinin geliştirilmesine yönelik önemli bilgiler sunmaktadır.

1. INTRODUCTION (GİRİŞ)

High energy density in electrochemical cells can be achieved either by increasing the specific capacity or by elevating the operating voltage. While high-voltage operation is an effective strategy, it is accompanied by critical challenges, including structural degradation of the cathode, instability at the cathode–electrolyte interface, and the electrolyte oxidation. These issues severely limit long-term performance, making the development of robust cathode materials and rational design strategies essential for achieving sustained cycling stability under high-voltage conditions [1, 2].

*Corresponding author, e-mail: bdkarahan@itu.edu.tr
DOI: 10.29109/gujsc.1850067

Currently, the predominant commercially used cathode chemistries are lithium iron phosphate (LFP), nickel manganese cobalt (NMC), and nickel cobalt aluminium (NCA). In addition, spinel lithium nickel manganese oxide (LNMO), lithium manganese oxide (LMO), and lithium manganese iron phosphate (LMFP) cathode chemistries have gained increasing attention due to their favourable cost-to-performance balance. Among these, spinel LNMO has emerged as a promising cathode material, offering a wide theoretical voltage window (3.0–4.75 V), three-dimensional lithium-ion transport pathways, and notable advantages in terms of cost and environmental impact compared to conventional layered oxide materials. However, capacity fading remains a major challenge for the long-term cycling stability of LNMO cathodes; therefore, further structural and chemical optimizations are required. The primary issues include oxidative decomposition of conventional electrolytes under high-voltage operation, structural degradation propagating from the surface into the bulk during repeated cycling due to volumetric changes, and Jahn–Teller lattice distortions associated with the presence of Mn^{3+} ions. [3, 4].

The formation of spinel phases with different space groups, namely disordered ($Fd\bar{3}m$) and ordered ($P4_332$), is strongly dependent upon the solid-state synthesis conditions. Particularly, precursor preparation and activation govern the resulting the powder's crystal defect formation, compositional homogeneity, and the emergence of intermediate phases through processing parameters such as ball milling conditions, mixing protocols, and mechanical activation in heat treatment. Subsequent heat treatment, including sintering or annealing, promotes ion mobility, enables atomic rearrangement via ordering or reordering processes, and ultimately drives phase transformation. Appropriate ball milling parameters can promote early-stage reactions and the formation of intermediate phases, thereby facilitating the subsequent formation of the spinel structure. Although mechanical activation can induce certain structural modifications, the degree of cation ordering and the stabilization of lower-symmetry spinel phases (e.g., $P4_332$) are predominantly governed by the thermal treatment conditions. Therefore, for better cathode performances a careful optimization of both ball milling parameters and calcination conditions is essential. After ball milling, calcination of LNMO powders below 700 °C leads to the formation of an ordered LNMO cathode with a tetragonal crystal structure ($P4_332$ space group). In this ordered spinel, Li^+ ions occupy the 8a tetrahedral sites, O^{2-} ions reside at the 24e and 8c sites, while Mn and Ni ions are preferentially located at the octahedral sites, respectively. This cation ordering is typically associated with a well-defined distribution of oxidation states, where Mn predominantly exists as Mn^{4+} with a minimal fraction of Mn^{3+}, and Ni is mainly present as Ni^{2+} with limited Ni^{3+} contribution. While such ordering enhances structural stability, the reduced Mn^{3+} content and restricted cation disorder can limit electronic conductivity and lithium-ion transport, resulting in comparatively lower electrochemical performance. In contrast, calcination at temperatures above 700 °C yields a disordered spinel phase with a face-centred cubic structure ($Fd\bar{3}m$ space group), in which Ni^{2+}/Ni^{3+} and Mn^{3+}/Mn^{4+} ions are randomly distributed over the octahedral (16d) and tetrahedral (8a) sites. This cation disorder promotes the partial reduction of Mn^{4+} to Mn^{3+} and the coexistence of mixed-valence Ni species, which collectively enhance electronic conductivity. Moreover, the disordered $Fd\bar{3}m$ structure provides open and continuous three-dimensional lithium-ion diffusion pathways, suppresses excessive interfacial impedance growth during cycling, and exhibits higher structural reversibility under deep delithiation conditions. Consequently, the $Fd\bar{3}m$ phase generally demonstrates improved electrochemical performance compared to its ordered counterpart, achieving a favourable balance between ionic conductivity, electronic transport, and structural stability. Zhang et al. [3] have seen ordered distribution of Mn and Ni below 700°C in air resulting poor cycling and rate performance. When calcination is realized at elevated temperatures (800–1000 °C), a predominantly disordered spinel LNMO structure is formed, which typically delivers enhanced electrochemical performance, particularly at high current densities. [3], [4].

During cycling, in the ordered structure, Li^+ ions migrate from the 8a tetrahedral sites to octahedral sites through a two-phase reaction mechanism characterized by distinct voltage plateaus. Such a biphasic transformation can generate lattice strain and structural stress, ultimately leading to diminished cycling stability. Moreover, Mn^{3+} ions are prone to Jahn-Teller distortion, leading to surface Mn dissolution and the formation of Mn_3O_4-like phases that hinder Li^+ diffusion and degrade rate performance. In contrast, the disordered spinel exhibits a solid-solution behavior with gradual changes in Li^+ concentration and no distinct phase separation, resulting in a smoother voltage profile over a wider range. The random cation distribution reduces structural stress and limits Mn_3O_4

formation, thereby disordered structure ($Fd\bar{3}m$) of LNMO performs better [9-11].

In the solid-state synthesis of LNMO, optimization of key processing parameters—such as ball-to-powder ratio (BPR), rotation speed (RPM), milling duration, filling ratio, and process control agent (PCA) content—is widely recognized as essential for achieving high structural integrity and improved cycling performance in cathode active materials. Despite this, comprehensive and systematic investigations that simultaneously examine the combined and interactive effects of all these critical parameters remain scarce in the literature [12] - [14]. Nevertheless, numerous studies have focused on improving cathode performance through surface engineering approaches, such as coatings with metal oxides, metal fluorides, or metal phosphates, as well as through elemental doping with metals, metalloids, or non-metals. Notably, boron—a non-metal element characterized by electron deficiency and a stronger B–O bond energy (809 kJ mol^{-1}) compared to Mn–O (402 kJ mol^{-1}) and Ni–O (380 kJ mol^{-1}) bonds—has been successfully incorporated into cathode materials such as LiV_3O_8 [8], [9], $LiCoO_2$ [10], [11], and $Li_{1.2}Mn_{0.6}Ni_{0.2}O_2$ [12], [13], substituting transition-metal sites and thereby improving their electrochemical performance. In 2021, Wei et al. [14] systematically investigated the influence of boron doping on the crystal structure, morphology, and kinetic behavior of LNMO, utilizing boric acid as the doping source at varying concentrations.

To the best of our knowledge, this study is the first to employ the Taguchi method for optimizing ball milling parameters in the synthesis of micron-sized, truncated octahedral LNMO particles. Micron-sized particles are preferred for LNMO production as they achieve an optimal balance between surface area and bulk properties, resulting in improved crystallinity, enhanced structural stability, and better lithium-ion diffusion and electrochemical kinetics. While very fine nanoparticles tend to aggregate and promote unwanted side reactions, excessively large particles hinder lithium-ion accessibility. Another critical characteristic for LNMO is the presence of (111) and (400) crystallographic planes within the $Fd\bar{3}m$ spinel structure, as the preferential exposure of these planes promotes effective lithium mobility and structural robustness due to their enhanced lithium diffusion pathways and structural stability [15].

Four critical parameters—ball-to-powder ratio, milling speed, milling time, and the weight percentage of ethanol as a process control agent (PCA)—were investigated at three levels, resulting in a total of nine experimental runs. Each experiment was conducted by processing the precursors according to the ball milling parameters defined by the L9 Taguchi design followed by thermal treatment at 800°C for 12 hours in an air atmosphere. 1st discharge capacity was taken as a response for the L9 design considering "Larger is better" approach. An additional control experiment was conducted to confirm the reliability and accuracy of the optimization. Analysis of variance (ANOVA) was performed to identify the most statistically significant parameter influencing LNMO synthesis via ball milling. Subsequently, under the optimized milling conditions, 1% boron was doped into the LNMO structure, and calcination at different temperatures (800 and 900 °C) applied to improve the capacity retention of boron-doped LNMO (B-LNMO800, and B-LNMO900). This study provides new insights into the synergistic effects of processing conditions and boron doping on the performance of LNMO cathode materials for lithium-ion batteries.

2. MATERIALS AND METHODS (MATERYAL VE METOD)

2.1. Powder Synthesis (Toz Sentezi)

The flowchart outlining the methodology adopted in this study is presented in Figure 1. First, nickel acetate (Alfa Aesar, CAS 6018-89-9) and manganese acetate (Alfa Aesar, CAS 6638-38-0) were subjected to ball milling with ethanol as a dispersing agent, following the L9 design. The resulting powder was then preheated at 480 °C for 4 h in air (Protherm). Subsequently, the predetermined amount of lithium hydroxide (in stoichiometric molar ratios of 0.5:1.5:1.05) and ethanol were added to the precursor and mixed overnight at 200 rpm without milling media in a planetary ball mill (Retsch PM 100). Following, the powder was dried under vacuum at 105 °C overnight and finally calcined at 800 °C for 12 hours in air to obtain the LMNO cathode active material. Finally, boron doping (B-LNMO ($Li_1Ni_{0.5}B_{0.01}Mn_{1.49}O_4$)) was made at the optimum ball milling conditions where boron trioxide (Sigma-Aldrich CAS 1303-86-2) was selected as the boron source. Afterwards, B-LNMO was heat treated at 800 °C and 900 °C for 12 hours (Fig. 1).

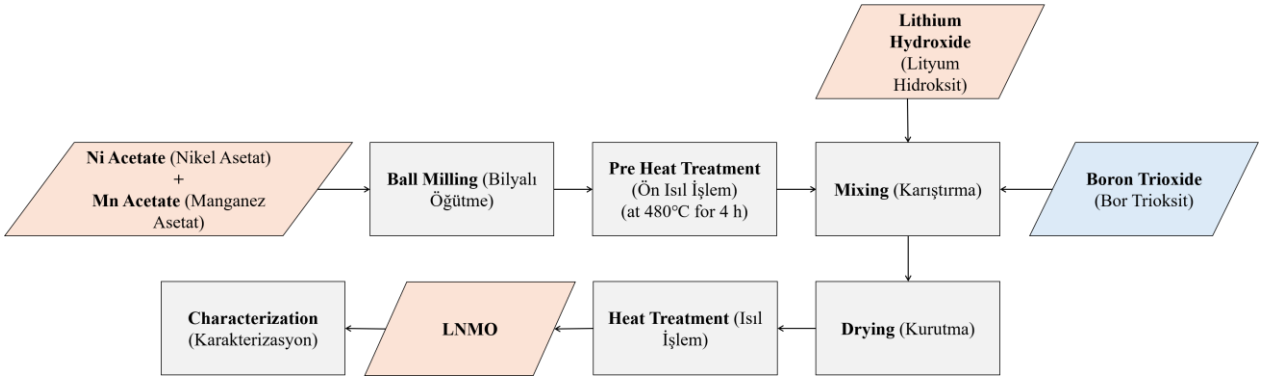

Figure 1. The schematic flow chart of the powder synthesis (Toz sentezinin şematik akış şeması)

2.2. Taguchi experimental design (Taguchi deney tasarımı)

For the optimization of four ball-milling parameters—namely ball-to-powder ratio, milling speed, milling time, and ethanol weight percentage—the Taguchi L9 (3^4) orthogonal array was employed, as presented in Table 1. The response factor was the 1st discharge capacity. Analysis was performed considering Taguchi's "Larger is better" approach using Minitab v16 (License Coord ID: 1178999).

Table 1. Parameters and their levels used in L9 design (L9 tasarımında kullanılan parametreler ve seviyeleri)

Trial No.	BPR (Ball to Powder)	Milling speed (RPM)	Milling time (h)	PCA (wt. %)
Sample 1	5	300	8	5
Sample 2	5	400	12	10
Sample 3	5	500	16	15
Sample 4	10	300	12	15
Sample 5	10	400	16	5
Sample 6	10	500	8	10
Sample 7	20	300	16	10
Sample 8	20	400	8	15
Sample 9	20	500	12	5

2.3. Structural, morphological and chemical characterization (Yapısal, morfolojik ve kimyasal karakterizasyon)

The fabricated powders were characterized comprehensively, the structural phases in the powder were analysed using X-ray diffraction (BRUKER, D2 Phaser) with a Cu Kα source between 10°-90° at a scanning speed of 0.5°/second. Phase quantification and in-depth assessment of lattice structure, parameters were realized by Rietveld refinement via Topas software v6.0. The particle shape and morphology were studied using scanning electron microscope (SEM, Zeiss Gemini 500). Further knowledge about the ordered-disordered crystal structure was explored by utilizing Raman Analysis (RENISHAW inVia and iRaman Plus 785H) with 785 nm laser source. The chemical composition of elements in the samples was studied by the inductive coupled plasma (ICP-MS 1500W, Agilent ICP 7700 Series, CA, USA).

2.4. Electrochemical characterization (Yapısal, morfolojik ve kimyasal karakterizasyon)

The cathodes were prepared by mixing of cathode active material, binder (polyvinylidene difluoride-PVDF, Gelon LIB Group), and a conductor agent (Timcal-C64) in weight ratios of 8:1:1 respectively using an appropriate amount of solvent (n-methyl-pyrrolidone-NMP, EMPLURA®). The slurry obtained was coated onto an aluminium foil (battery grade) with 150 µm wet thickness using doctor blade. The electrodes were dried then calendared. The cells were assembled using a 16 mm cathode electrode, a polypropylene separator (Celgard 2400), a 12 mm lithium electrode, and a 1:1 ratio of ethylene carbonate (EC) and dimethyl carbonate (DMC) containing a 1 M lithium hexafluorophosphate (LiPF6) solution in glovebox (MBraun, LABmaster Pro). For electrochemical performance characterization, electrodes were tested in a galvanostatic charge-discharge station (Neware Battery Analyzer) in the 3V-4.8V range, at current loads of 0.1 C (14.7 mA/g). Cyclic voltammetry tests were performed on the Gamry Interface 1000E at a scan rate of 0.1 mV/s in the 3V-4.8V range. To investigate changes in impedance,

electrochemical impedance spectroscopy (EIS) was carried out at 3V, from 0.01 Hz to 100 kHz (Gamry Interface1000E) in symmetrical cells. The symmetric cells were assembled following the procedure suggested by Burns et al. [16], to eliminate the interference from metallic Li during impedance testing. The EIS parameters were fitted using Gamry software (Echem Analyst 2).

3. RESULTS (BULGULAR)

3.1. Optimization of ball milling conditions to sythesize disordered structured micron sized LNMO (Düzensiz yapılı mikron boyutlu LNMO sentezi için bilyalı öğütme koşullarının optimizasyonu)

Following the L_9 (3^4) Taguchi design of experiment, total 9 experiments were conducted. Figure 2 indicates the XRD pattern of the samples, revealing that all samples have disordered LNMO structure of standard spinel Fdm space group (PDF # 01-082-8899). Couple of peaks matched to the trigonal (R3m) $Li_{0.58}Ni_{1.04}O_2$ phase peaks, according to literature, the formation of this impurity could be resulted from non-uniform mixing of precursors and/or oxygen loss at high temperatures (≥ 800°C) [17]. The lattice parameters and phase distribution in each sample is calculated based on Rietveld refinement method given in Table 2.

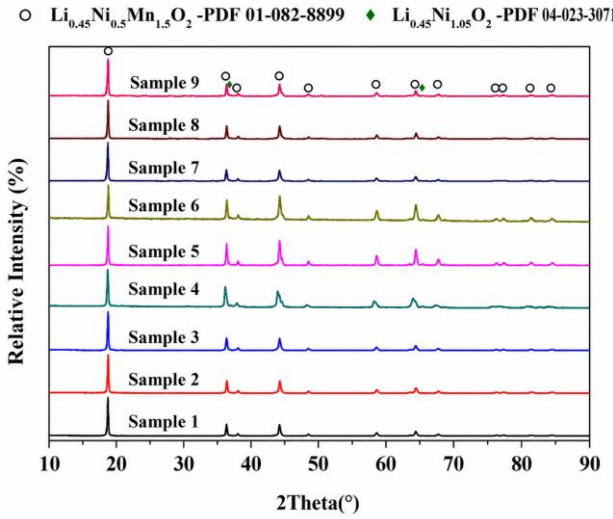

Figure 2. XRD pattern of the 9 experiments (9 deneyin XRD deseni)

The intensity ratio of the (111) peaks to the (311) is examined to determine the {111} surface orientation (Table 2). Sample 1 has the highest ratio. {111} surface orientation prevails the preferred exposure of the {111} facets combined with a disordered structure which enhances the structural stability while inhibiting Mn-dissolution. This surface orientation also accelerates the Li^+ diffusion while simultaneously inhibiting the volumetric strain during charge/discharge cycle. The high crystallinity of the spinel structure is indicated by the minimum width at the half-maximum of the (400) peak. The higher the value is the better the crystallinity as in the case of sample 4 [18]. Plus, sample 4 has the largest lattice parameters, which implies that the amount of Mn^{+3} in sample 4 may be higher (because its ionic radius is larger than that of Mn^{+4}).

Table 2. Lattice parameters, I(111)/I(311), FWHM (400) of the experiments (Deneylerin kafes parametreleri, I(111)/I(311), FWHM (400))

Trials	Lattice parameter (Å)	$I_{(111)}/I_{(311)}$	$FWHM_{(400)}$
sample 1	8.1692	2.70	0.274
sample 2	8.1675	2.24	0.283
sample 3	8.1738	2.19	0.304
sample 4	8.213	1.57	0.359
sample 5	8.1709	1.52	0.255
sample 6	8.164	1.15	0.331
sample 7	8.1691	2.69	0.318
sample 8	8.1648	2.24	0.264
sample 9	8.1692	2.36	0.265

The morphologies of all the samples consist of both submicron and micron-sized truncated octahedral particles along with rectangular particles, but sample 1 has more homogenous particle distribution (Fig. 3a) as compared to the others. It is worth highlighting that when milling speed and time is at their low levels (i.e., 300 RPM and 8 h, respectively), particle agglomeration is minimum. Additionally, the octahedral morphology in sample 1 confirms the highest {111} surface orientation (see Figure 2). Sample 2 (Fig. 3b) comprises of majorly rectangular and fewer octahedral-shaped particles. Sample 3 (Fig. 3c) shows relatively larger micron-sized particles as compared to others due to long milling duration and the highest milling speed. Samples 4-7 (Fig. 3d-g) reveal a heterogeneous particle size distribution (micron and submicron size) of octahedral and rectangular particles, along with a severe agglomeration especially in sample 6. In Sample 8, nano-sized particles are predominant, and discontinuous octahedral particles at the micron level are also observed. In Sample 9, particles of varying sizes, mostly octahedral in structure, are obtained.

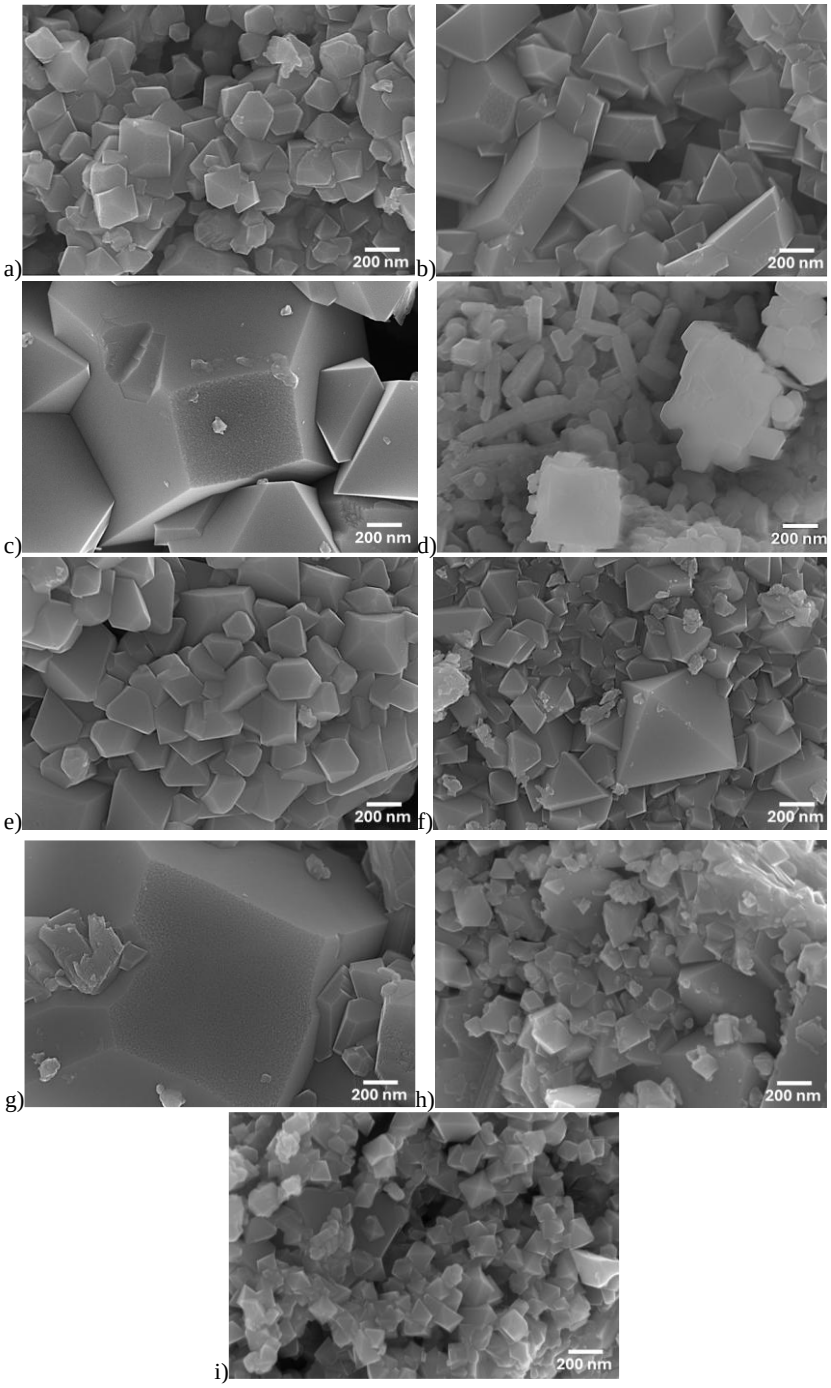

Figure 3. SEM images of sample a) 1, b) 2, c) 3, d) 4, e) 5, f) 6, g) 7, h) 8, i) 9 (Numunelerin SEM görüntüleri: a) 1, b) 2, c) 3, d) 4, e) 5, f) 6, g) 7, h) 8, i) 9)

Raman analyses give insight of vibration mode between Ni^{+2} and O^{-2} at 408 and 499 cm^{-1} (E_2 and F_{2g} bands) (Fig. 4). The vibration of Mn^{+4} and Mn^{+3} with O is in the 595–640 cm^{-1} range (A_{1g} band), this band is used to determine the ordered and disordered structure [19]. In theory, the appearance of two well-defined Raman active modes at approximately 595 and 612 cm^{-1} are considered as a signature of a long-range ordered arrangement of Ni and Mn cations within the LNMO lattice structure [19]. Unlikely, in the present study, the absence of distinct peaks in this spectral region indicates a lack of cation ordering in all nine synthesized LNMO samples proving their disordered cubic spinel structure [20]. Additionally, the low intensity of the peaks at 164 cm^{-1} also confirms the presence of the disordered spinel structure in all 9 samples.

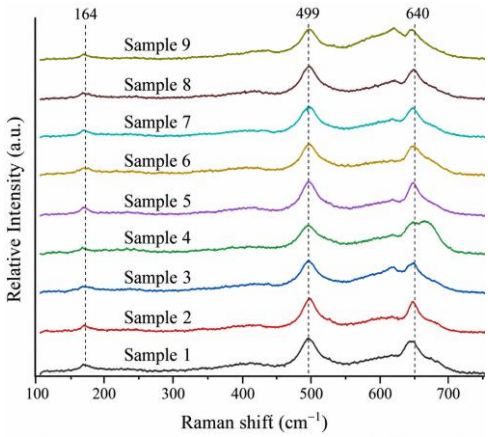

Figure 4. Raman shifts of the 9 experiments (9 deneyin Raman kaymaları)

Then, galvanostatic test results of these 9 samples are studied to discuss the effect of ball milling conditions on the electrochemical performances of LNMO particles (Figure 5a-c). The formation of a plateau at 4V emphasizes the existence of disordered structure, where nickel and manganese are randomly positioned at the 16d sites. Additionally, lower initial coulombic efficiency (in the range of 70-80%) is observed in the first cycle of each spinel structure (Fig. 5c). This could be explained by the destabilization of the electrochemical inactive layer formed at the cathode-electrolyte interface during lithium ion deintercalation, and/or Mn^{3+} disproportionation, and/or rock-salt impurities formed by nickel migration to the surface. These factors prevent the return of Li^+ ions to the host structure [21]. The sample 4 shows the lowest discharge capacity due to having Mn^{+3} in the lattice which also leads to the highest lattice parameter. The relatively larger ionic radius of Mn^{+3} causes the lattice elongation that eventually imparts reduced mobility of Li ions, structural instability and capacity fading [22]. Sample 1 exhibits the highest initial discharge capacity because the {111} crystallographic orientation, which hosts the transition metals, has low surface energy that suppresses cathode–electrolyte side reactions, thereby reducing cathode degradation compared to other orientations. In addition, the more uniform distribution of micron- and submicron-sized particles helps mitigate degradation throughout the cathode, from the surface to the bulk.

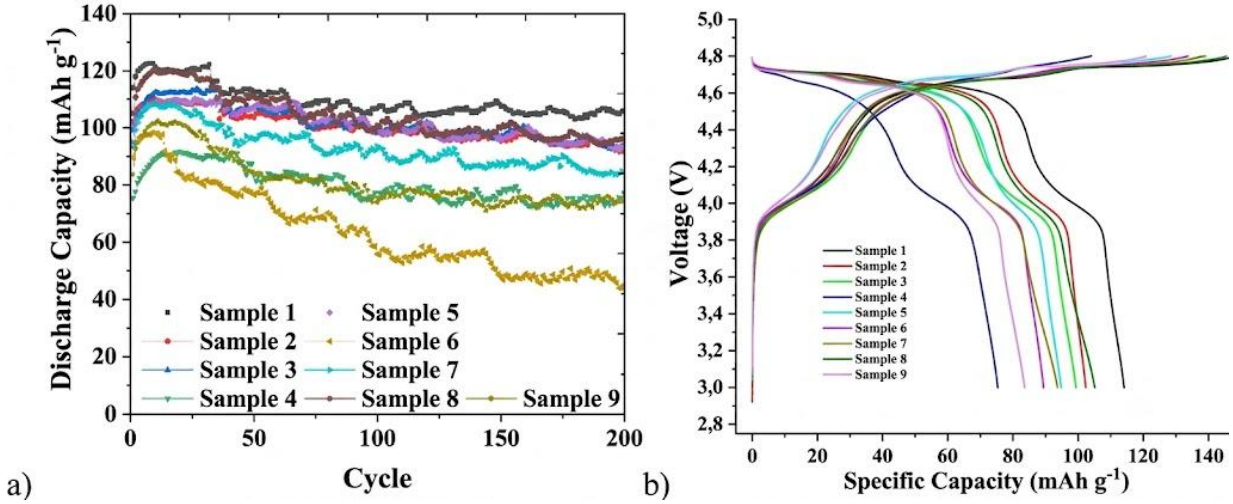

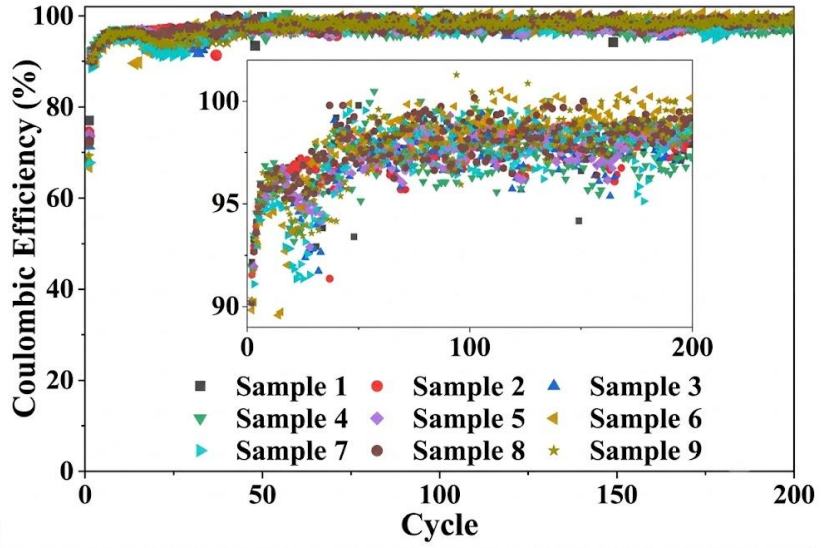

c)

Figure 5. Galvanostatic test results of the 9 experiments at 0.1C a) Capacity- cycle graph, Galvanostatic test results of the 9 experiments at 0.1C a) Capacity- cycle graph, b) Voltage-capacity graph c) Coulombic Efficiency-cycle graph (0,1C'de yapılan 9 deneyin galvanostatik test sonuçları: a) Kapasite-çevrim grafiği, b) voltaj-kapasite grafiği, c) Coulomb verimliliği-çevrim grafiği)

In the analysis of Taguchi L9 design, the initial discharge capacities are taken as the output (Table3). "The Larger is Better" approach is used in the optimization.

Table 3. The 1st discharge capacities of the nine experiments from Taguchi L9 (Taguchi L9'dan elde edilen dokuz deneyin ilk deşarj kapasiteleri)

Trials	BPR	Milling speed (RPM)	Milling time (h)	PCA (Wt. %)	1st Discharge Capacity
sample 1	5	300	8	5	114.0
sample 2	5	400	12	10	102.3
sample 3	5	500	16	15	99.3
sample 4	10	300	12	15	75.4
sample 5	10	400	16	5	94.8
sample 6	10	500	8	10	89.4
sample 7	20	300	16	10	93.7
sample 8	20	400	8	15	105.1
sample 9	20	500	12	5	83.6

Figure 6 shows the S/N ratio plot of the milling parameters, it is clear that the highest S/N can be obtained when the milling conditions are set to BPR 5, at 400 RPM for 8 h. The least effective parameter is found to be the wt. % ethanol is . Therefore, the predicted value (by Taguchi) of the initial discharge capacity prepared at the best conditions (BPR 5, milling time 8 h, milling speed 400 rpm) calculated to be 118.2 mAh/g.

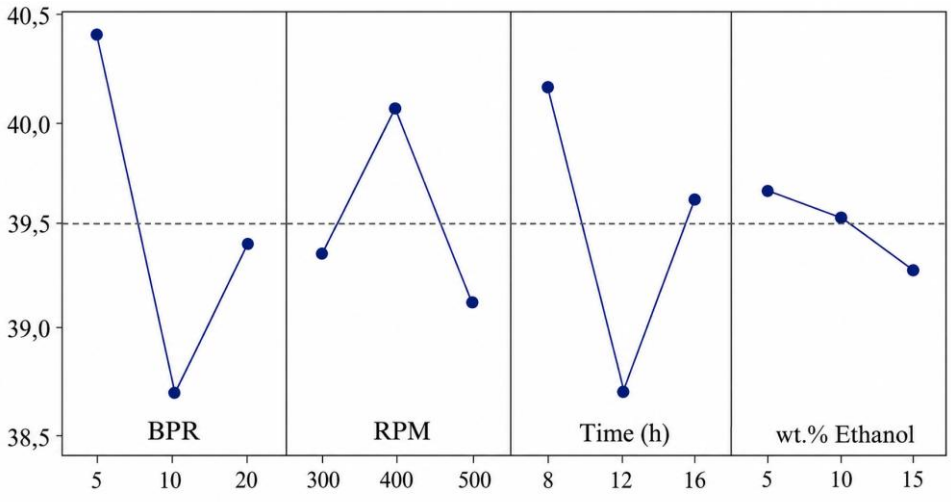

Figure 6. Main effect plot of the milling parameters to S/N (Öğütme parametrelerinin S/N'ye olan ana etki grafiği)

To validate the best experiemntal conditions, a control experiment (sample 10) is conducted. The same heat treatment procedure (at 800°C for 12 hours in air) is applied to synthesize disordered structured spinel LNMO. In the control experiment, the initial charge capacity was obtained as 145.9 mAh/g, and the discharge capacity was obtained as 110.5 mAh/g. The first-cycle Coulombic efficiency was found 75.7%, similar to the results in the experimental set. Since calculated discharge capacity is 118.2 mAh/g, there is a 93% accuracy in between predicted versus the control experiment.

Finally, in ANOVA analysis, since the effect of ethanol amount is not as significant as the others its variance is pooled and R^2 and $R^2_{(adjusted)}$ values are calculated to be 97.55% and 90.2% showing very high model confidence.

Table 4. Analysis of Taguchi experimental design (Taguchi deney tasarımının analizi.)

Level	BPR	Milling speed (RPM)	Milling time (h)	Ethanol (wt.%)
1	40.43	39.37	40.2	39.71
2	38.7	40.06	38.73	39.55
3	39.44	39.14	39.64	39.31
Total	118.57	118.57	118.57	118.57
Delta (variation)	1.72	0.92	1.47	0.40
Rank (Significance)	1	3	2	4

Table 5. Pooled Analysis of variance (ANOVA) (Havuzlanmış varyans analizi (ANOVA))

Parameters	df	Sum of squares	Contributions (%)	F	p-
BPR	2	529.87	48.91	19.96	0.048
Milling speed (RPM)	2	152.79	14.1	5.76	0.148
Milling time (h)	2	374.24	34.54	14.10	0.066
Error	2	26.55	2.45		
Total	8	1083.45	100		

3.2. Optimization of calcination temperatures to synthesize disordered structured 1% Boron doped LNMO cathode (Düzensiz Yapılı %1 Bor Katkılı LNMO Katotunun Sentezi için Kalsinasyon Sıcaklıklarının Optimizasyonu)

To investigate the effect of calcination temperature upon doping, a new set of experiments is conducted in which the precursor of Sample 10 is mixed with B_2O_3 to achieve 1% boron doping and then calcined at 800°C (B-LNMO800) and 900°C (B-LNMO900) for 12 hours in air. B-LNMO800 consists of micron-sized particles with octahedral morphology and a {111} surface orientation (Fig. 7a–c). In contrast, B-LNMO900 exhibits larger particles with a mixture of octahedral and rectangular shapes. As expected, higher temperature promotes the particle growth.

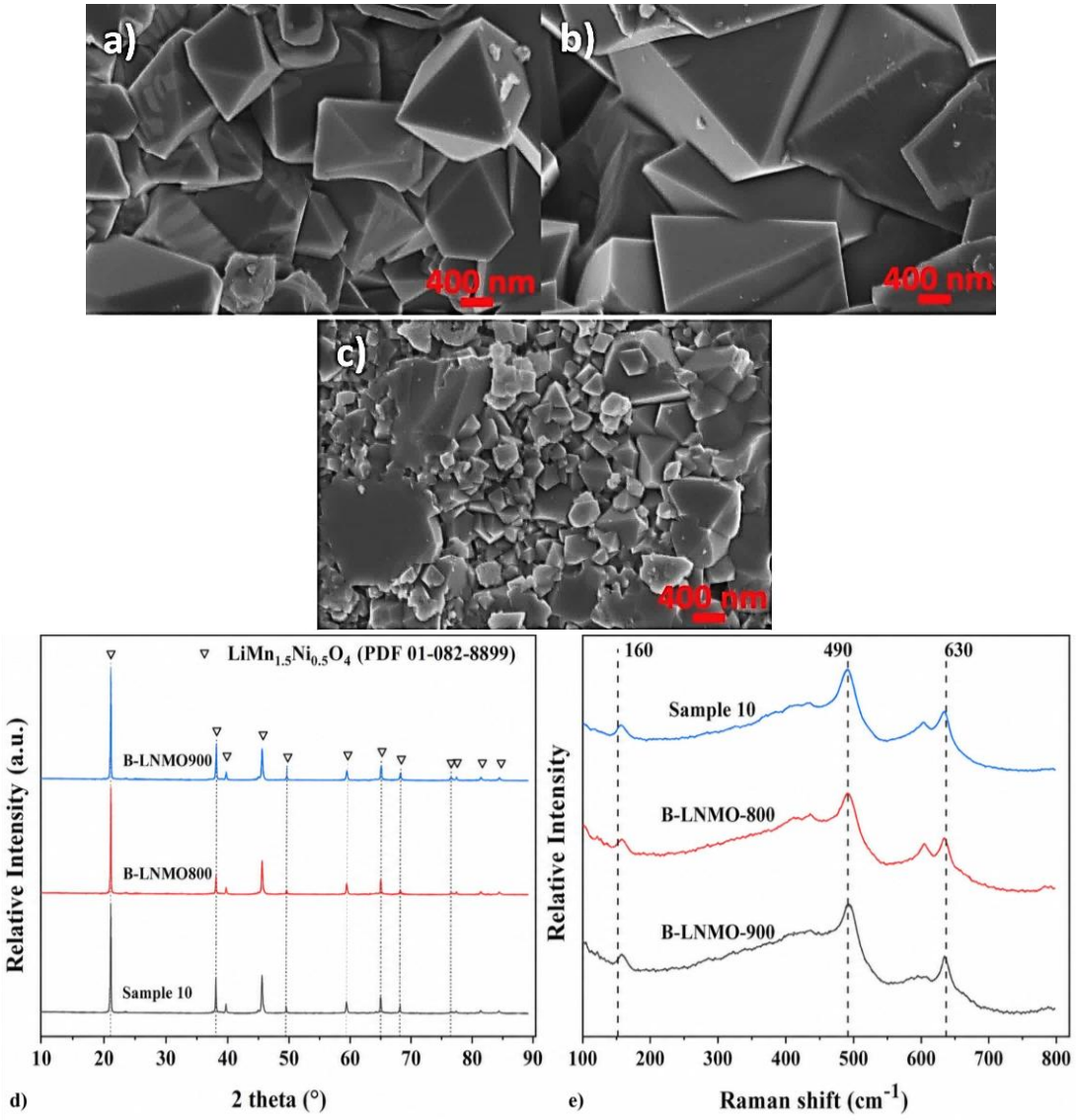

Figure 7. SEM images of a) B-LNMO800, b) B-LNMO900, c) sample 10, d) XRD pattern, e) Raman spectra (a) B-LNMO800, b) B-LNMO900, c) numune 10'un SEM görüntüleri, d) XRD deseni, b) Raman spektrumları)

The XRD pattern of sample 10 shows the existence of LNMO with spinel $Fd\bar{3}m$ space group (PDF 01-082-8899). Fig. 7d shows that higher calcination temperatures promote the decomposition of the main LNMO phases, resulting in an increased formation of undesirable secondary phases at 2θ = 36.9°, and 65.59° [23]. And, the high-energy bond formed between boron and oxygen in the structure prevents the oxygen release from the structure [24]. Raman spectroscopy analyses of the sample 10, B-LNMO800 and B-LNMO900 samples yield similar Raman shift peaks, (595 and 612 cm^{-1}) with indistinct bump-shaped curves, indicating that the crystal structure is predominantly disordered. The low intensity peak at 160 cm^{-1}, in all the 3 samples also affirms the existence of disordered spinel structure.

The surface reactions are investigated via cyclic voltammetry (CV) shown in Fig. 8, the formation of a bump at 4 V for all three samples indicates the occurrence of Mn redox reaction (Eq. 1). The more pronounced bump observed for the B-LNMO900 sample indicates a higher concentration of Mn^{3+} ions in its structure compared to the other samples. Furthermore, the redox reactions associated with Ni occur at approximately 4.7 V and ~4.75 V, as described in Equations (2) and (3), respectively. From the second cycle onward, the voltage profiles of all three samples nearly overlap, indicating highly similar electrochemical behaviour. This convergence suggests that the reactions become more reversible after the initial cycle, leading to improved capacity retention in subsequent cycles.

$$Mn^{+3} \leftrightarrow Mn^{+4} \quad (1)$$

$$Ni^{+2} \leftrightarrow Ni^{+3} \quad (2)$$

$$Ni^{+3} \leftrightarrow Ni^{+4} \quad (3)$$

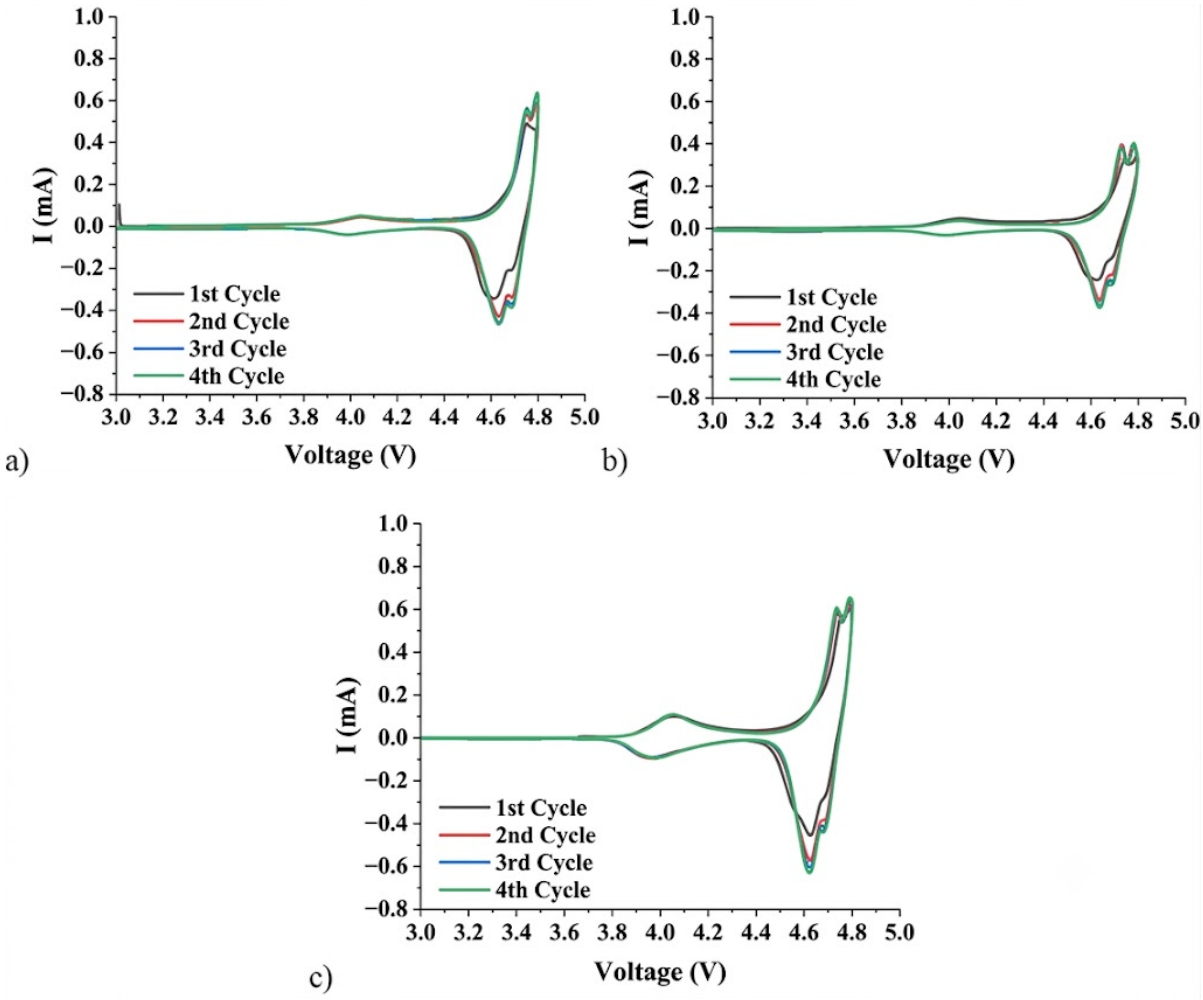

Figure 8. Cyclic voltammetry results of a) Sample 10, b) B-LNMO800, c) B-LNMO900 (a) Numune 10, b) B-LNMO800, c) B-LNMO900'ün döngüsel voltametri sonuçları)

Fig. 9 reveals the electrochemical performance of the three samples and the initial discharge capacities (at 0.1C) are found to be as 110.4 mAh/g, 63.34 mAh/g and 97.3 mAh/g for sample 10 (verification experiment), B-LNMO800 and B-LNMO900, respectively. The corresponding columbic efficiencies (at 0.1C) are determined as 75.7%, 64.1%, and 81.1%, respectively. After 130 cycles, sample 10 delivers 92.7 mAh/g, while B-LNMO800 and B-LNMO900 perform 68.6 and 97.5 mAh/g, respectively. By these electrochemical results it can be inferred that owing to enhanced bond energy of boron with oxygen, the structural stability is improved. The boron addition partially prevents the dissolution of manganese and nickel from the structure due to electrolyte oxidation at high voltage (in a completely delithiated state) [14], [25]. Furthermore, boron restricts rock-salt impurity formation during high-temperature calcination, reducing electrochemical inactivity on the cathode surface and facilitating the transportation of lithium ions into the structure which eventually enhances

the columbic efficiency [26]. The obtained enhanced electrochemical performance of LNMO is comparable to the prior reported performances [27].

Herein, it is worth emphasizing that for B-LNMO800 the capacity delivered is lower than that of sample 10 (Fig. 9), this could be assigned to inadequate mixing of boron precursor prior to calcination forming a glassy film covering the particle surface to limit the interaction of the active particle with the electrolyte, resulting in lower current in CV [28]. The performance comparison of the samples with the perior literature, is provide in Table 6.

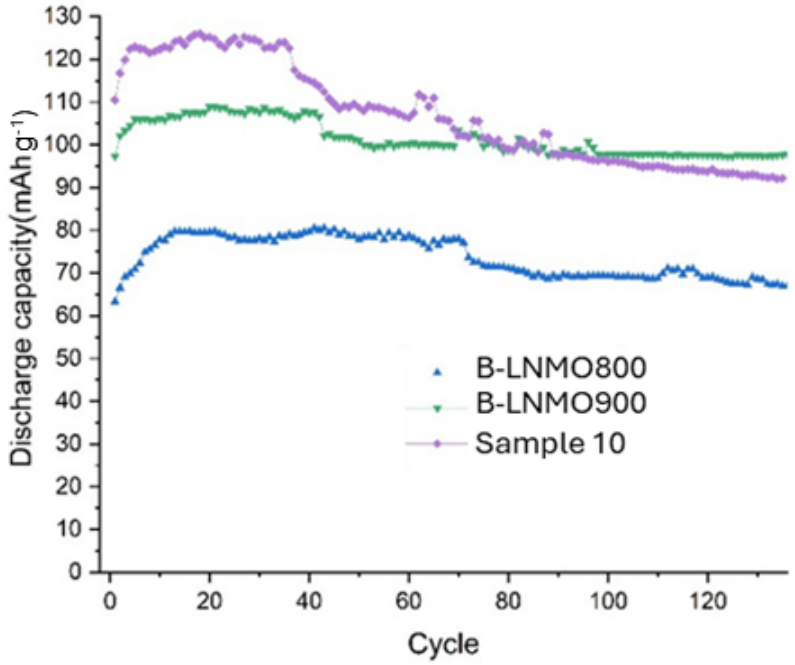

Figure 9. Capacity-Cycle plot of B-LNMO800, B-LNMO900 and Sample 10 at 0.1C (B-LNMO800, B-LNMO900 ve Numune 10'un 0,1°C'deki Kapasite-Çevrim grafiği)

Table 6. Performance Comparison of LNMO cathode with literature (LNMO katodunun literatürle performans karşılaştırması)

Reference	Current Load (C) (1C = 147mA g-1)	Cycle	Specific Capacity (mAh g-1)
[29]	0.1C	3	~125
[30]	0.1C	5	130
[31]	0.1C	5	~125
This Study	0.1C	130	97.5

To further validate the mechanism of calcination upon %1B doping at different temperatures, EIS of the electrodes (B-LNMO800, B-LNMO900, and sample 10) after 1st and 3rd discharge at 3 V was realized. The electrolyte resistance is found to be approximately 2-2.5 Ω for all three samples. Impedance against Li^+ movement at the cathode-electrolyte interface is observed in the high-frequency region for all three samples, as well as charge transfer impedance and linear Warburg impedance in the mid-frequency region.

The similar charge transfer resistance observed in the first and third cycles for the B-LNMO900 sample indicates the formation of a stable cathode-electrolyte interface after the first cycle, with the lowest value (~8.5 Ω) compared to the others. And the higher charge transfer resistance observed in the

first and third cycles for the B-LNMO800 sample confirms the existence of glassy film over the particle surface. The EIS results of the three samples (after 1st and 3rd cycle) and the fitted model are given in Fig. 10a-d.

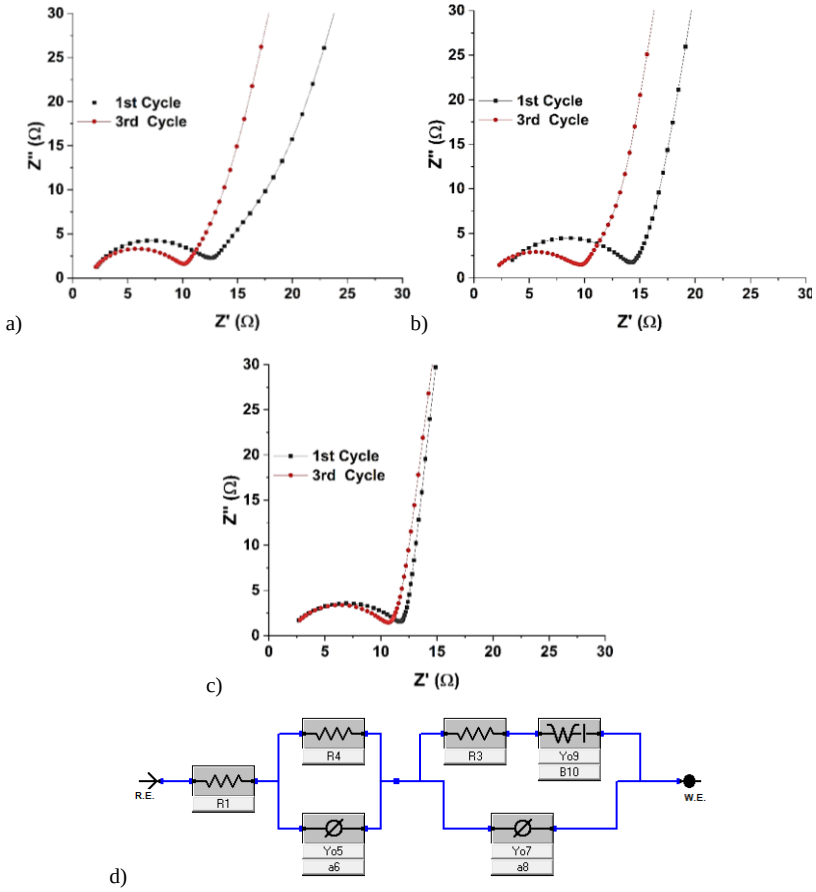

Figure 10. EIS spectra of a) Sample 10, b) B-LNMO800, c) B-LNMO900 d) Fitted Model (a) Numune 10, b) B-LNMO800, c) B-LNMO900 ve d) Uyumlu Modelin EIS spektrumları)

4. CONCLUSIONS (SONUÇLAR)

In this study, the effects of ball-to-powder ratio, milling speed, milling time, and ethanol content as a process control agent on LNMO synthesis were systematically investigated using Taguchi L9 design. The analysis revealed BPR 5, milling time 8 h, milling speed 400 rpm had the most significant impact on the initial discharge capacity. Optimization of the milling conditions enabled the successful synthesis of LNMO with enhanced electrochemical performance. Furthermore, the introduction of 1% boron into the LNMO structure, followed by calcination at 800 and 900 °C, improved capacity retention, demonstrating the synergistic effect of optimized processing and boron doping. These findings provide valuable insights for the design and development of high-performance LNMO cathodes for lithium-ion batteries and suggest that careful control of processing parameters combined with strategic doping can effectively enhance battery performance.

ACKNOWLEDGMENTS (TEŞEKKÜR)

The study is funded by ITU Scientific Research Project Unit (Project No. 45208). The authors acknowledge gratefully REMER (Istanbul Medipol University) for XRD, SEM analysis. Moreover, special thanks to Metrohm for Raman.

DECLARATION OF ETHICAL STANDARDS (ETİK STANDARTLARIN BEYANI)

The author of this article declares that the materials and methods they use in their work do not require ethical committee approval and/or legal-specific permission.

Bu makalenin yazarı çalışmalarında kullandıkları materyal ve yöntemlerin etik kurul izni ve/veya yasal-özel bir izin gerektirmediğini beyan ederler.

AUTHORS' CONTRIBUTIONS (YAZARLARIN KATKILARI)

***Yunus Emre GÜL*:** Investigation, methodology, visualization, writing – original draft.

Araştırma, metodoloji, görselleştirme, yazım – orijinal taslak.

***Humza ASHRAF*:** Validation, writing – original draft.

Doğrulama, yazma – orijinal taslak.

***Billur Deniz KARAHAN*:** Conceptualization, writing – original draft, supervision.

Kavramsallaştırma, yazım – orijinal taslak, denetim

CONFLICT OF INTEREST (ÇIKAR ÇATIŞMASI)

There is no conflict of interest in this study.

Bu çalışmada herhangi bir çıkar çatışması yoktur.

REFERENCES (KAYNAKLAR)

[1] Y. Zhang *et al.*, "Research Development on Spinel Lithium Manganese Oxides Cathode Materials for Lithium-Ion Batteries," *J. Electrochem. Soc.*, vol. 170, no. 9, p. 090532, Sep. 2023, doi: 10.1149/1945-7111/ACF8FD.

[2] J. H. Kim, N. P. W. Pieczonka, and L. Yang, "Challenges and Approaches for High-Voltage Spinel Lithium-Ion Batteries," *ChemPhysChem*, vol. 15, no. 10, pp. 1940–1954, Jul. 2014, doi: 10.1002/CPHC.201400052.

[3] L. Zhang, L. Yin, X. Zhang, and N. T. Ruiz, "Structural and Electrochemical Investigation of High Energy Spinel LiMn1.5Ni0.5O4 Produced at Low Temperature," *ECS Meet. Abstr.*, vol. MA2021-01, no. 2, p. 144, May 2021, doi: 10.1149/MA2021-012144MTGABS.

[4] B. Y. Lee, C. T. Chu, M. Krajewski, M. Michalska, and J. Y. Lin, "Temperature-controlled synthesis of spinel lithium nickel manganese oxide cathode materials for lithium-ion batteries," *Ceram. Int.*, vol. 46, no. 13, pp. 20856–20864, Sep. 2020, doi: 10.1016/J.CERAMINT.2020.05.124.

[5] Y. Wang *et al.*, "Effect of Mn3O4 particle size on synthesis and electrochemical performance of spinel LiMn2O4 cathode," *Ionics (Kiel).*, vol. 31, no. 8, pp. 7745–7755, Aug. 2025, doi: 10.1007/S11581-025-06441-8/FIGURES/7.

[6] M. Xu *et al.*, "Enabling structural and interfacial stability of 5 V spinel LiNi0.5Mn1.5O4 cathode by a coherent interface," *J. Energy Chem.*, vol. 76, pp. 266–276, Jan. 2023, doi: 10.1016/J.JECHEM.2022.09.021.

[7] M. A. Kebede, N. Palaniyandy, L. F. Koao, F. I. Ezema, and M. R. Mhlongo, "Current Status and Trends in Spinel Cathode Materials for Lithium-Ion Battery," *Electrode Mater. Energy Storage Convers.*, pp. 35–46, Sep. 2021, doi: 10.1201/9781003145585-3.

[8] P. Mei *et al.*, "LiV3O8 nanorods as cathode materials for high-power and long-life rechargeable lithium-ion batteries," *RSC Adv.*, vol. 4, no. 49, pp. 25494–25501, Jun. 2014, doi: 10.1039/C4RA02269F.

[9] Y. Niu *et al.*, "Cathode Materials Based on LiV3O8 Nanostructures for Sodium-Ion Batteries," *ACS Appl. Nano Mater.*, vol. 6, no. 1, pp. 622–632, Jan. 2022, doi: 10.1021/ACSANM.2C04736.

[10] J. Li, R. Zhao, X. He, and H. Liu, "Preparation of LiCoO2 cathode materials from spent lithium-ion batteries," *Ionics (Kiel).*, vol. 15, no. 1, pp. 111–113, Feb. 2009, doi: 10.1007/S11581-008-0238-8.

[11] J. H. Shim *et al.*, "Characterization of Spinel LixCo2O4-Coated LiCoO2 Prepared with Post-Thermal Treatment as a Cathode Material for Lithium Ion Batteries," *Chem. Mater.*, vol. 27, no. 9, pp. 3273–3279, May 2015, doi: 10.1021/ACS.CHEMMATER.5B00159.

[12] K. lin Cheng, D. bin Mu, B. rong Wu, L. Wang, Y. Jiang, and R. Wang, "Electrochemical performance of a nickel-rich LiNi0.6Co0.2Mn0.2O2 cathode material for lithium-ion batteries under different cut-off voltages," *Int. J. Miner. Metall. Mater.*, vol. 24, no. 3, pp. 342–351, Mar. 2017, doi: 10.1007/S12613-017-1413-6.

[13] F. Cheng, Y. Xin, J. Chen, L. Lu, X. Zhang,

and H. Zhou, "Monodisperse Li1.2Mn0.6Ni0.2O2 microspheres with enhanced lithium storage capability," *J. Mater. Chem. A*, vol. 1, no. 17, pp. 5301–5308, May 2013, doi: 10.1039/C3TA00153A.

[14] A. Wei *et al.*, "Enhancing electrochemical performance and structural stability of LiNi0.5Mn1.5O4 cathode material for rechargeable lithium-ion batteries by boron doping," *Ceram. Int.*, vol. 47, no. 1, pp. 226–237, Jan. 2021, doi: 10.1016/J.CERAMINT.2020.08.125.

[15] M. E. Donets *et al.*, "Mechanical Milling Effect on Structural and Electrochemical Properties of Cathode Material," *PPNL*, vol. 19, no. 5, pp. 532–535, Oct. 2022, doi: 10.1134/S1547477122050156.

[16] J. C. Burns *et al.*, "Introducing Symmetric Li-Ion Cells as a Tool to Study Cell Degradation Mechanisms," *J. Electrochem. Soc.*, vol. 158, no. 12, p. A1417, Nov. 2011, doi: 10.1149/2.084112JES/XML.

[17] Sudaryanto *et al.*, "Comparison of lithium sources on the electrochemical performance of LiNi0.5Mn1.5O4 cathode materials for lithium-ion batteries," *Int. J. Renew. Energy Dev.*, vol. 13, no. 3, pp. 448–456, May 2024, doi: 10.61435/ijred.2024.59662.

[18] J. Karunawan, P. N. Suryadi, L. Mahfudh, S. P. Santosa, A. Sumboja, and F. Iskandar, "Truncated Octahedral Shape of Spinel LiNi0.5Mn1.5O4 via a Solid-State Method for Li-Ion Batteries," *Energy & Fuels*, vol. 37, no. 1, pp. 754–762, Jan. 2022, doi: 10.1021/ACS.ENERGYFUELS.2C03507.

[19] G. Oney *et al.*, "Identification of degree of ordering in spinel LiNi0.5Mn1.5O4 through NMR and Raman spectroscopies supported by theoretical calculations," *Energy Storage Mater.*, vol. 70, p. 103486, Jun. 2024, doi: 10.1016/J.ENSM.2024.103486.

[20] J. H. Kim *et al.*, "Investigation of Ordering on Oxygen-Deficient LiNi0.5Mn1.5O4-δ Thin Films for Boosting Electrochemical Performance in All-Solid-State Thin-Film Batteries," *Small*, vol. 18, no. 24, p. 2201134, Jun. 2022, doi: 10.1002/SMLL.202201134;WGROUP:STRING:PUBLICATION.

[21] N. P. W. Pieczonka *et al.*, "Understanding Transition-Metal Dissolution Behavior in LiNi0.5Mn1.5O4 High-Voltage Spinel for Lithium Ion Batteries," *J. Phys. Chem. C*, vol. 117, no. 31, pp. 15947–15957, Aug. 2013, doi: 10.1021/JP405158M.

[22] S. Sun *et al.*, "Magnetic Field-induced Disordered Phase of Spinel Oxides for High Battery Performance," *Adv. Mater.*, vol. 36, no. 35, p. 2405876, Aug. 2024, doi: 10.1002/ADMA.202405876.

[23] J. Liu *et al.*, "Insight into the interplay of the additive and different calcination process for the cobalt-free high voltage spinel LiNi0.5Mn1.5O4 cathode," *Nano Energy*, vol. 140, p. 111038, Jul. 2025, doi: 10.1016/J.NANOEN.2025.111038.

[24] N. R. Park *et al.*, "Understanding the Role of Lithium Borate as the Surface Coating on High Voltage Single Crystal LiNi0.5Mn1.5O4," *Adv. Funct. Mater.*, vol. 34, no. 13, p. 2312091, Mar. 2024, doi: 10.1002/ADFM.202312091.

[25] J. Yang, X. Han, X. Zhang, F. Cheng, and J. Chen, "Spinel LiNi0.5Mn1.5O4 cathode for rechargeable lithiumion batteries: Nano vs micro, ordered phase (P4332) vs disordered phase (Fd$\bar{3}$m)," *Nano Res.*, vol. 6, no. 9, pp. 679–687, Jul. 2013, doi: 10.1007/S12274-013-0343-5/METRICS.

[26] Y. Luo *et al.*, "Improved long cycle performance of LiMn2O4 cathode material by Ni-B co-doping combined with truncated octahedron morphology," *J. Alloys Compd.*, vol. 924, p. 166537, Nov. 2022, doi: 10.1016/J.JALLCOM.2022.166537.

[27] T. Kocak *et al.*, "Effect of doping amount on capacity retention and electrolyte decomposition of LiNi0.5Mn1.5O4-based cathode at high temperature," *J. Solid State Chem.*, vol. 310, p. 123006, Jun. 2022, doi: 10.1016/J.JSSC.2022.123006.

[28] C. Du *et al.*, "Surface modification of a LiNi0.5Mn1.5O4 cathode with lithium boron oxide glass for lithium-ion batteries," *RSC Adv.*, vol. 5, no. 71, pp. 57293–57299,

Jun. 2015, doi: 10.1039/C5RA06271C.

[29] D. Versaci *et al.*, "Tailoring cathode materials: A comprehensive study on LNMO/LFP blending for next generation lithium-ion batteries," *J. Power Sources*, vol. 613, no. 17, p. 234955, Sep. 2024, doi: 10.1016/j.jpowsour.2024.234955.

[30] P. Guan *et al.*, "High-rate LiNi0.5Mn1.5O4 cathode materials for Li-ion batteries by the strategy of multi-ion co-doping," *Chem. Eng. J.*, vol. 516, p. 163892, Jul. 2025, doi: 10.1016/j.jechem.2019.08.022.

[31] S. Pazhaniswamy *et al.*, "Ceramic–Polymer–Carbon Composite Coating on the Truncated Octahedron-Shaped LNMO Cathode for High Capacity and Extended Cycling in High-Voltage Lithium-Ion Batteries," *Energy & Fuels*, vol. 38, no. 21, pp. 21456–21467, Nov. 2024, doi: 10.1021/acs.energyfuels.4c02933.